Short Communications

J. Synchrotron Rad. (1999). **6**, 112–115

X-ray powder diffraction with hybrid semiconductor pixel detectors

S. Manolopoulos,[a] R. Bates,[a] G. Bushnell-Wye,[b] M. Campbell,[c] G. Derbyshire,[d] R. Farrow,[b] E. Heijne,[c] V. O'Shea,[a] C. Raine[a] and K. M. Smith[a]*

[a]Department of Physics and Astronomy, University of Glasgow, Glasgow, UK, [b]CLRC Daresbury Laboratory, Warrington, Cheshire, UK, [c]ECP Division, CERN, Geneva, Switzerland, and [d]CLRC Rutherford Appleton Laboratory, Didcot, Oxfordshire, UK. E-mail: k.smith@physics.gla.ac.uk

(*Received 24 September 1998; accepted 21 January 1999*)

Semiconductor hybrid pixel detectors, originally developed for particle physics experiments, have been used for an X-ray diffraction experiment on a synchrotron radiation source. The spatial resolution of the intensity peaks in the diffraction patterns of silicon and potassium niobate powder samples was found to be better than that of a scintillator-based system, typically used at present. The two-dimensional position information of the pixel detector enabled multi-peak diffraction patterns to be acquired and clearly resolved without the need for an angle scan with a diffractometer. This trial experiment shows the potential of this technology for high-resolution high-rate diffraction systems.

Keywords: semiconductor pixel detectors; X-ray diffraction imaging; photon counting.

1. Introduction

Semiconductor pixel detectors were initially developed for high-energy-physics applications because of their low noise, high granularity, stand-alone pattern recognition capabilities, good spatial resolution and true two-dimensional position information (Heijne, 1988; Parker, 1989; Damerell, 1995; Kemmer & Lutz, 1988; Karchin, 1991). It was soon realized that these characteristics would lend themselves to X-ray imaging applications (Hall, 1995; Breskin, 1997; Fischer *et al.*, 1998) and that semiconductor pixel detectors could replace traditionally used systems such as radiographic film in medical applications. For synchrotron radiation applications, which also require fast efficient detectors with good spatial resolution and a large dynamic range, the true two-dimensional position information is a bonus which awaits exploitation. The construction of new bright synchrotron sources, such as the DIAMOND project in the UK, with photon energies from 3–60 keV and very high X-ray fluxes provided by insertion devices on third-generation machines, imposes even more stringent criteria on the choice of detector.

Active pixel sensors (APS) are hybrid semiconductor detectors in which the detector, segmented into a two-dimensional array with metal electrodes, makes electrical contact with a geometrically matching array of front-end readout electronics channels by means of metallic bonds of approximately spherical shape (bump bonds). This gives great flexibility in the design, since it allows the separate optimization of the detector and readout integrated circuit (ROIC). For the former, semiconductor materials with a higher atomic number than silicon can be used, for example GaAs or CdTe, with the aim of increasing the X-ray detection efficiency (Matherson *et al.*, 1998; Butler *et al.*, 1998; Manolopoulos *et al.*, 1998). For the latter, the advantages of VLSI technology in the fabrication of application-specific integrated circuits (ASIC) can be fully exploited in the design to provide a substantial amount of 'logic' in the front-end electronics at the pixel level.

The Ω3 ROIC was initially developed to be hybridized with a matching array of silicon detectors for high-energy-physics applications (Heijne *et al.*, 1996). It consists of a matrix of 2048 (128 × 16) pixels with a pixel size of 50 μm × 500 μm and operates in the pulse-counting mode. The circuitry of the individual pixel cell consists of a preamplifier, shaper amplifier, discriminator, counting elements and elements for testing or masking purposes. Recently its performance as an X-ray imaging device was evaluated, both with Si and with GaAs as the detecting media (Manolopoulos *et al.*, 1998). As an indication of the potential of such detectors, Fig. 1 shows the X-ray detection efficiency and the modulation transfer function measured along the narrower pixel dimension. In the work reported here, the performance of an Ω3 ROIC bonded to a 'standard' 300 μm-thick high-resistivity silicon detector was evaluated in powder XRD experiments.

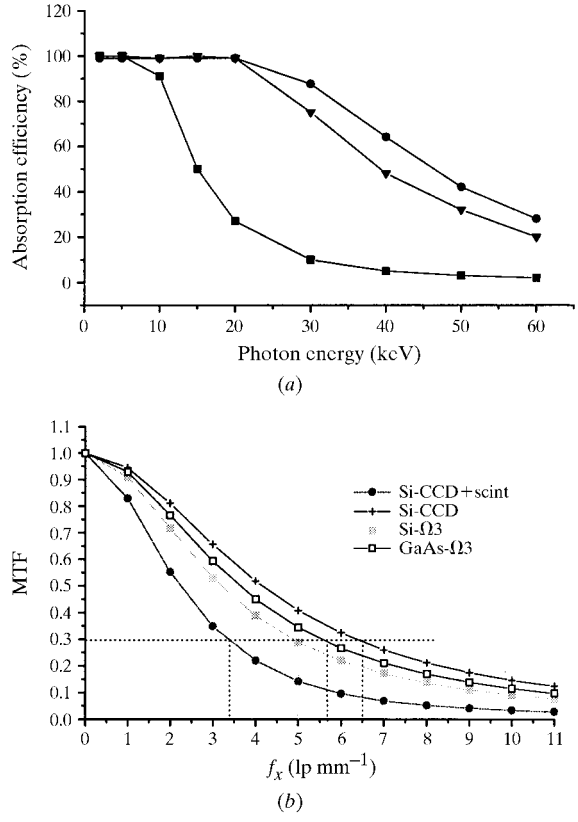

Figure 1
(*a*) X-ray detection efficiency for 300 μm-thick Si (squares), 200 μm- and 300 μm-thick GaAs (triangles and circles, respectively); (*b*) Measured MTF for Ω3 ROIC coupled to 300 μm-thick Si and to 200 μm-thick GaAs compared with commercial Si CCD and scintillator-coated Si CCD used in dental imaging.

2. X-ray diffraction powder method

In Debye–Scherrer geometry, a monochromatic X-ray beam is scattered by the crystal planes of a fine powder sample contained in a capillary tube. Because of the random orientations of the crystallites in the samples, the diffracted rays emerge on a cone at an angle of 2θ with respect to the original beam direction. This will be projected as a ring onto a film placed normal to the incident beam direction, or a series of concentric rings for all the crystal planes that satisfy the Bragg condition.

In recent years, film has been replaced by a variety of electronic detectors, ranging from gaseous MWPC to scintillators. In the latter case, if no positional information is provided, an angular scan is needed across an arc with the specimen at its vertex in order to detect the rings and form the diffraction pattern. Image plates (storage phosphors) are also used extensively as two-dimensional detectors but these introduce other limitations such as image decay, an additional scanning process before the data can be displayed and erasure time.

2.1. *Silicon sample*

Fig. 2 shows an example of the diffraction pattern of a silicon powder sample inserted into the path of a 25.523 keV X-ray beam at the synchrotron radiation facility in Daresbury (UK). The detector used was a scintillator disk of diameter 20 mm with its effective area reduced by means of a 300 μm-wide slit collimator placed directly in front of the scintillator, connected to a standard readout chain of photomultiplier, amplifier, discriminator and counter. The distance from the detector to the sample was ∼600 mm. The diffraction pattern was produced by scanning across the 2θ range from 8.25 to 9.25° in steps of 0.01°. As shown in Fig. 2, a single peak appears at an angle 2θ of 8.88° with a spatial resolution, defined as the full width of the peak at half the maximum count (FWHM), of 0.033°, corresponding to 346 μm.

The scintillator system was replaced by the Ω3 pixel detector, at the same distance from the sample and at such an angle that the silicon diffraction peak appeared at approximately the middle of the matrix. The discriminator threshold was set to ∼24 keV. A background run was first taken with no beam illumination of the sample, to mask the noisy pixels. It was followed by a data-collecting run, with identical beam settings to those in the scintillator experiment. The diffraction pattern can be seen in Fig. 3(*a*). The two-dimensional information of the pixel detector obviates the need for an angle scan, since the ring that corresponds to the diffraction peak at 8.88° can easily be seen as an arc across the pixel matrix. The mean spatial resolution across the 16 columns spanning the arc is found in this case to be 257 μm [Fig. 3(*b*)]. (The small 'hot spot' at the upper left of the image is due to a noisy pixel that escaped the masking procedure, as identified by a background run taken immediately after the XRD measurement.)

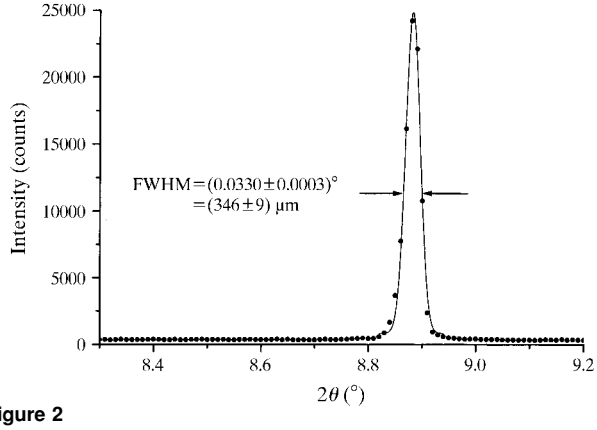

Figure 2
XRD pattern of Si powder across the 111 reflection, taken with a scintillator detector. The beam energy was 25.5 keV.

2.2. *Potassium niobate sample*

The same experiment was repeated with a potassium niobate (KNbO3) powder sample replacing the silicon, with the objective of testing the ability of the pixel detector in resolving complex multi-peaked diffraction patterns. Once more the scintillator

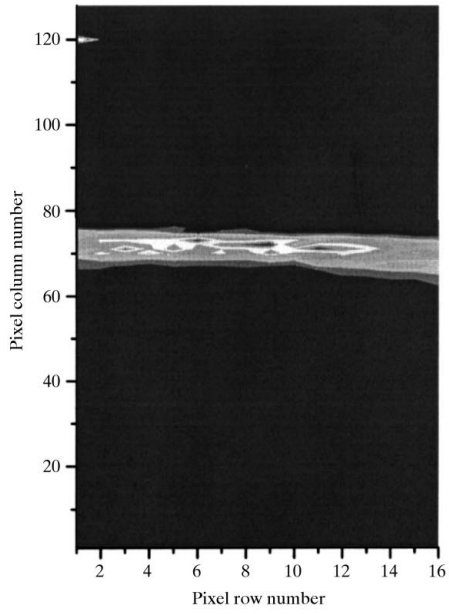

(*a*)

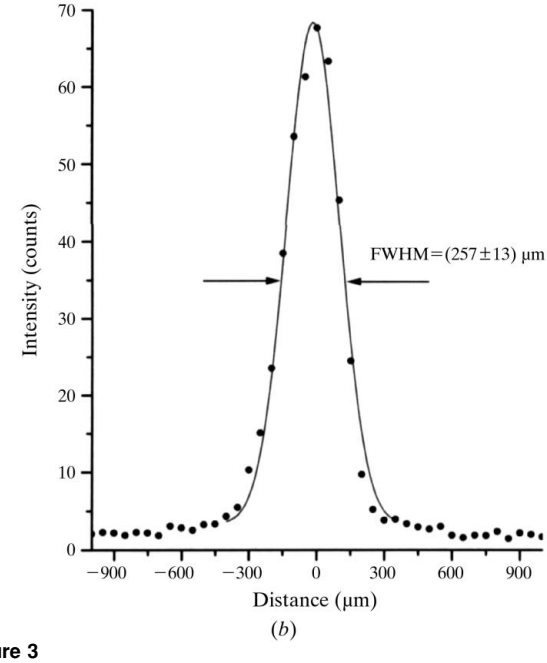

(*b*)

Figure 3
XRD pattern of Si powder across the 111 reflection, taken with an Ω3 Si pixel detector. The beam energy was 25.5 keV. See text.

detector was used first to record the diffraction pattern, for comparison purposes. Fig. 4 shows the full diffraction pattern for a 2θ scan from 6° to 15°. The triple peak at ∼9.8° was identified as the obvious candidate to be resolved by the pixel detector.

Accordingly, the diffraction pattern of the KNbO3 powder was taken with the Ω3 Si detector placed at a 2θ angle of ∼9.8° [Fig. 3(*a*)]. The peaks can be easily resolved, as shown also in Fig. 3(*b*), with the additional facility of two-dimensional spatial information provided by this detector. Finally, for the KNbO3 diffraction pattern taken with the pixel detector, Fig. 3(*c*), the peak-to-valley ratio was 6.1 (2.1) for the main (secondary) peaks.

3. Conclusions and future work

An active pixel sensor incorporating silicon as the detection medium was used in powder X-ray diffraction experiments. It was

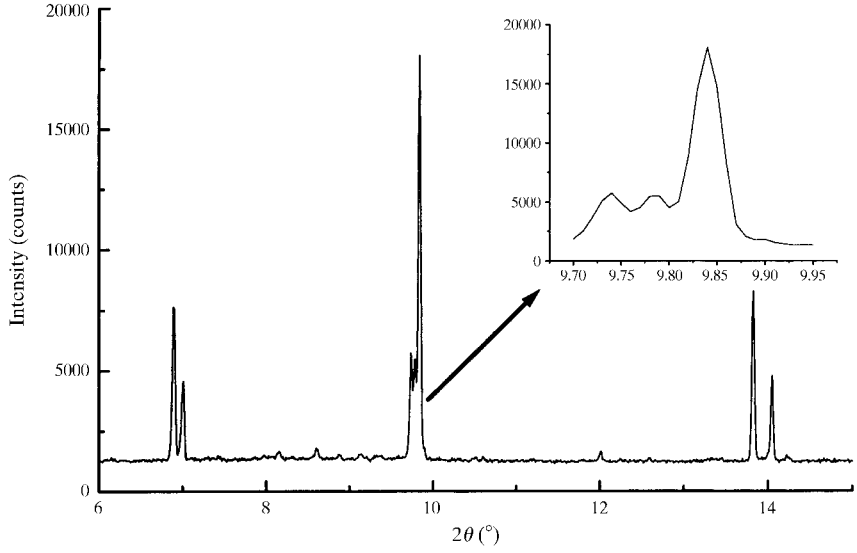

Figure 4
XRD pattern of KNbO3 powder, taken with a scintillator detector. The beam energy was 25.5 keV.

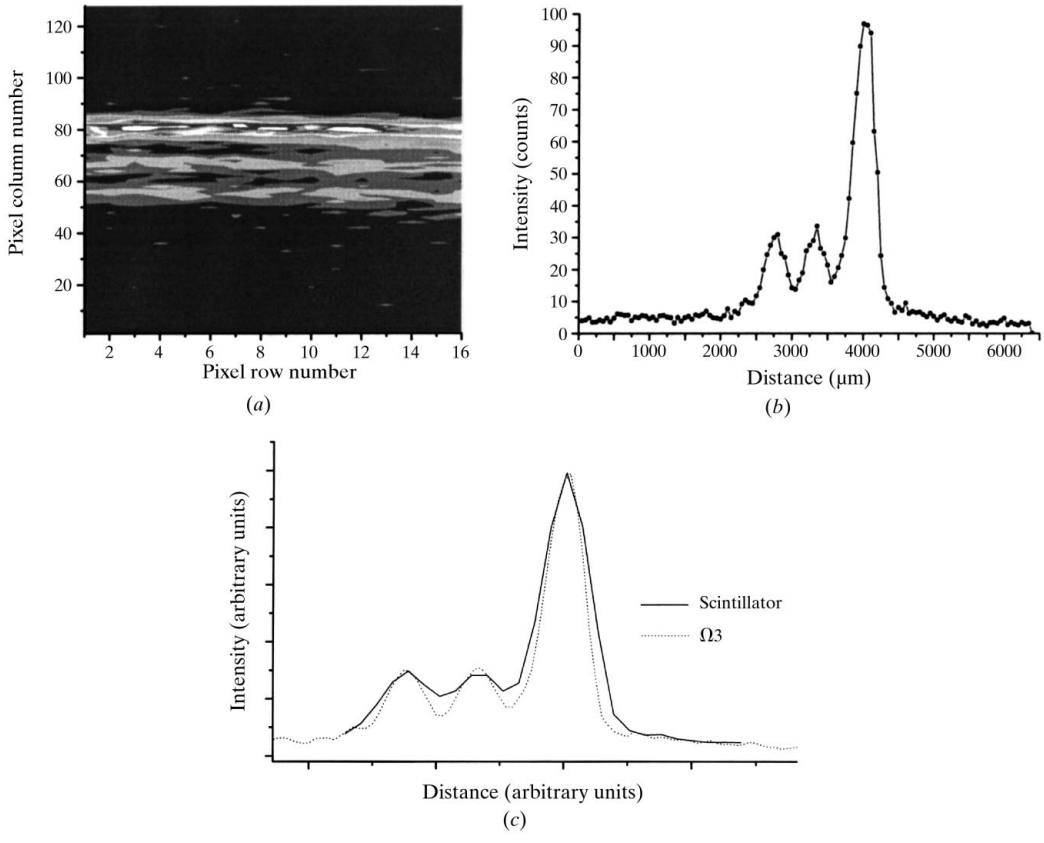

Figure 5
(*a*) XRD pattern of KNbO3 powder, taken with an Ω3 Si pixel detector. The beam energy was 25.5 keV. (*b*) Projection along a column. (*c*) Comparison with the scintillator data.

found that the spatial resolution can be superior to a current system, due to the small pixel electrode dimensions which are easily obtainable with the photolithographic techniques commonly used in the fabrication of semiconductor detectors. In our case, the pixel pitch was 50 μm. The improved spatial resolution results in a better peak-to-valley ratio in the diffraction patterns. Although of limited extent, this trial experiment has shown that an open-face pixel detector can provide clear improvements in data quality. An array of similar detectors would prove to be an extremely useful detector as a scanning diffractometer would be unnecessary. This type of detector could also be used in single-crystal XRD which requires the accurate measurement of position and intensity of discrete spots in a two-dimensional plane.

The number of counts accumulated in the diffraction patterns taken with the pixel detector is, however, orders of magnitude less than those taken with the scintillator detector (see, for example, Figs. 2 and 3). This is primarily due to operation of the chip in a synchronous mode, *i.e.* pulses are registered as hits only when in coincidence with an external clock pulse. Each pixel readout is therefore active only for the ($\leq$4 μs) width of the trigger pulse during every readout cycle of 8.3 ms, resulting in an active fraction of $\sim 5 \times 10^{-4}$ and a dead time as high as 99.94% (Manolopoulos *et al.*, 1998).

A new development from this ROIC is the MEDIPIX (Campbell *et al.*, 1998), which incorporates a 15-bit pseudorandom counter on each 170 μm × 170 μm pixel and operates in a shutter-based mode, *i.e.* all pulses that exceed the discriminator threshold are registered within a pre-set time window. This chip should overcome the dead-time limitations of the Ω3 mentioned above and enable data-acquisition rates of $\sim$1 MHz pixel^{-1}. A new series of XRD experiments to verify this behaviour, as well as the large dynamic range and short frame readout time [measured electrically as 384 μs on a 10 MHz clock (Campbell *et al.*, 1998)], is planned for the near future at the synchrotron radiation facility of Daresbury Laboratory (UK). Finally, the response across the whole dynamic range is expected to be linear, as already found with the Ω3 (Manolopoulos *et al.*, 1998), but it will still be necessary to investigate whether the noise performance is photon-statistics limited, unlike the Ω3 Si and Ω3 GaAs systems described above.

This work was undertaken as part of the IMPACT (UK Foresight) programme. It developed from our participation in the RD19 (Pixel Detector R&D) collaboration, supported by the CERN Laboratory (Campbell *et al.*, 1990), which supplied the Ω3 ROIC. The authors would also like to extend their thanks to Bob Cernik of the SRS at Daresbury for his support and interest in this project.

References

Breskin, A. (1997). *Nucl. Instrum. Methods*, A**387**, 1–18.

Butler, J. F., Lingren, C. L., Friesenhahn, S. J., Doty, F. P., Ashburn, W. L., Conwell, R. L., Augustine, F. L., Apotovsky, B., Pi, B., Collins, T., Zhao, S. & Isaacson, C. (1998). *IEEE Trans. Nucl. Sci.* **45**, 359–363.

Campbell, M., Heijne, E. H. M., Jarron, P., Krummenacher, F., Enz, C. C., Declercq, M., Vittoz, E. & Viertel, G. (1990). *Nucl. Instrum. Methods*, A**290**, 149–157.

Campbell, M., Heijne, E. H. M., Meddeler, G., Pernigotti, E. & Snoeys, W. (1998). *IEEE Trans. Nucl. Sci.* **45**, 751–753.

Damerell, C. (1995). Report RAL-P-95-008. Rutherford Appleton Laboratory, Didcot, Oxfordshire.

Fischer, P., Hausmann, J., Overdick, M., Raith, B., Wermes, N., Blanquart, L., Bonzom, V. & Delpierre, P. (1998). *Nucl. Instrum. Methods*, A**405**, 53–59.

Hall, G. (1995). *Q. Rev. Biophys.* **28**, 1–25.

Heijne, E. H. M., Jarron, P., Olsen, A. & Redaelli, N. (1988). *Nucl. Instrum. Methods*, A**273**, 615–619.

Heijne, E. H. M., Antinori, F., Barberis, D., Becks, K. H., Beker, H., Beusch, W., Burger, P., Campbell, M., Cantatore, E., Catanesi, M. G., Chesi, E., Darbo, G., D'Auria, S., Da Via, C., Di Bari, D., Di Liberto, S., Gys, T., Humpston, G., Jacholkowski, A., Jaeger, J. J., Jakubek, J., Jarron, P., Klempt, W., Krummenacher, F., Knudson, K., Kubasta, J., Lassalle, J. C., Leitner, R., Lemeilleur, F., Lenti, V., Letheren, M., Lisowski, B., Lopez, L., Loukas, D., Luptak, M., Metinengo, P., Meddeler, G., Meddi, F., Middelkamp, P., Morando, M., Morettini, P., Munns, A., Musico, P., Pellegrini, F., Pengg, F., Pospisil, S., Quercigh, E., Ridky, J., Rossi, L., Safarik, K., Scharfetter, L., Segato, G., Simone, S., Smith, K., Snoeys, W., Sobczynski, C., Stastny, J. & Vrba, V. (1996). *Nucl. Instrum. Methods*, A**383**, 55–63.

Karchin, P. (1991). *Nucl. Instrum. Methods*, A**305**, 497–503.

Kemmer, J. & Lutz, G. (1988). *Nucl. Instrum. Methods*, A**273**, 588–598.

Manolopoulos, S., Bates, R., Campbell, M., Da Via, C., Heijne, E., Heuken, M., Jurgensen, H., Ludwig, J., Marder, D., Mathieson, K., O'Shea, V., Raine, C., Rogalla, M. & Smith, K. M. (1998). *IEEE Trans. Nucl. Sci.* **45**, 394–400.

Matherson, K. J., Barber, H. B., Barrett, H. H., Eskin, J. D., Dereniak, E. L., Marks, D. G., Woolfenden, J. M., Young, E. T. & Augustine, F. L. (1998). *IEEE Trans. Nucl. Sci.* **45**, 354–358.

Parker, S. (1989). *Nucl. Instrum. Methods*, A**275** 494–516.